JACS
JOURNAL OF THE AMERICAN CHEMICAL SOCIETY
Communication
pubs.acs.org/JACS

Metal–Organic Frameworks as Platforms for the Controlled Nanostructuring of Single-Molecule Magnets

Darpandeep Aulakh,[†,∥] Joshua B. Pyser,[†,∥] Xuan Zhang,[‡] Andrey A. Yakovenko,[§] Kim R. Dunbar,[‡] and Mario Wriedt*[,†]

[†]Department of Chemistry & Biomolecular Science, Clarkson University, Potsdam, New York 13699, United States
[‡]Department of Chemistry, Texas A&M University, College Station, Texas 77845, United States
[§]X-ray Science Division, Advanced Photon Source, Argonne National Laboratory, Argonne, Illinois 60439, United States

Supporting Information

ABSTRACT: The prototypical single-molecule magnet (SMM) molecule $[Mn_{12}O_{12}(O_2CCH_3)_{16}(OH_2)_4]$ was incorporated under mild conditions into a highly porous metal–organic framework (MOF) matrix as a proof of principle for controlled nanostructuring of SMMs. Four independent experiments revealed that the SMM clusters were successfully loaded in the MOF pores, namely synchrotron-based powder diffraction, physisorption analysis, and in-depth magnetic and thermal analyses. The results provide incontrovertible evidence that the magnetic composite, SMM@MOF, combines key SMM properties with the functional properties of MOFs. Most importantly, the incorporated SMMs exhibit a significantly enhanced thermal stability with SMM loading advantageously occurring at the periphery of the bulk MOF crystals with only a single SMM molecule isolated in the transverse direction of the pores.

The magnetic properties of single-molecule magnets (SMMs) and their origins have been described in numerous detailed reviews.[1−3] As a key feature, the combination of a large spin ground state and high axial magnetic anisotropy in these molecules results in a barrier for the spin reversal and, therefore, the observation of slow magnetization relaxation rates below a threshold temperature value, attributed to purely molecular origin rather than long-range ordering. These characteristics enable the smallest data storage element to be as tiny as a single molecule, which would represent a breakthrough from the empirical Kryder's law, predicting a doubling of the data storage density every 13 months.[4] The current maximum density to date is approximately 200 Gbit cm^{-2}, whereas the upper limit by using single molecules is predicted to be 30 Tbit cm^{-2}.[5] Many of the forecast practical application of SMMs, however, will require their organization into 2D or 3D networks to allow for read-and-write processes,[6] which is a challenge given that SMM molecules are often decomposed under conditions required to obtain ordered arrays. Specifically they need to be protected from the environment to retain their unique magnetic properties.

In general, lithographic techniques are well adapted to the goal of isolating nanostructures of a few hundred molecules, but to attain the ultimate density one would have to rely on self-assembly processes of these molecules. Several approaches to the nanostructuring of SMMs have recently been reviewed,[7−9] including their association on surfaces[7,8] as well as their incorporation into carbon nanotubes[10,11] and mesoporous silicas.[12−15] All of these composite materials share the common feature that that the nanostructures are restricted to a more short-range order and that they also raise questions regarding their stability and processability.[16,17] Thus, the controlled long-range organization of SMMs in different dimensionality architectures while remaining in a protected chemical environment continues to be a major challenge in this research field.

Metal–organic frameworks (MOFs) are crystalline porous materials composed of metal clusters connected by polytopic organic linkers.[18,19] Due to their well-ordered multidimensional cavities, MOFs have the potential to be excellent hosts to achieve a precise long-range assembly of guest molecules for the fabrication of functional hybrid magnetic materials. In fact they have been shown to be excellent candidates for various composite[20] and device[21] fabrications and can serve as a container for nanoparticles which constitutes a physical bridge between the nanoscopic and macroscopic worlds.[22] To our knowledge, however, no examples of molecular magnets inserted in MOFs have been reported to date.

In this study we selected a host–guest model system with the prototypical SMM molecule $[Mn_{12}O_{12}(O_2CCH_3)_{16}(OH_2)_4]$ or $Mn_{12}Ac$ (**1**)[23,24] as the guest molecule and the mesoporous aluminum-based MOF $[Al(OH)(SDC)]_n$ (H_2SDC = 4,4′-stilbenedicarboxylic acid)[25] or CYCU-3 (**2**) as the host framework. The $Mn_{12}Ac$ molecule is by far the most well-studied SMM to date and exhibits a blocking temperature of 4 K. Its shape can be described as a 1.1 × 1.6 nm discoid (Figure 1A). The MOF CYCU-3 consists of hexagonal 1D channel pores of ∼3 nm diameter (Figure 1B) with high thermal and solvent stability. These characteristics indicate that **2** is well suited for hosting $Mn_{12}Ac$ with the added advantage that the diamagnetic aluminum centers will not influence the overall SMM properties of $Mn_{12}Ac$. Both precursors are readily obtained by low-cost and straightforward syntheses and their crystalline nature allows for the use of modern synchrotron-based X-ray diffraction techniques to analyze their structural

Received: June 9, 2015
Published: July 13, 2015

DOI: 10.1021/jacs.5b06002
J. Am. Chem. Soc. 2015, 137, 9254−9257

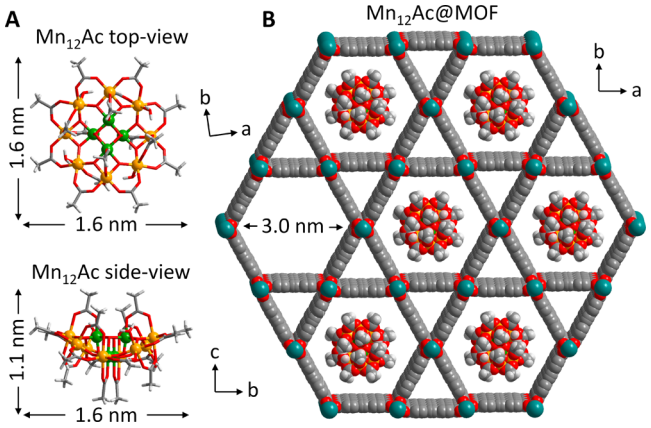

Figure 1. (A) Wireframe structure of $[Mn_{12}O_{12}(O_2CCH_3)_{16}(OH_2)_4]$ (**1**) and its dimensions. (B) Schematic representation of CYCU-3 (**2**) with guest molecules of **1**. Structures are shown in a spacefilling style with realistic size relationship between the atoms. Color scheme: manganese(IV), green; manganese(III), orange; aluminum, turquoise; carbon, gray; oxygen, red; and hydrogen, white.

properties. The latter is a significant advantage over other reported amorphous mesoporous silica composites.[13,14]

At the same time, interesting magnetic compounds have been derived from SMMs used as nodes in 1D−3D MOFs.[26−30] The development of this new material class has been similarly pushed by efforts on the nontrivial organization of SMMs. However, instead we present a new, alternative approach of using MOFs as platform for the nanostructuration of SMMs in a post-synthetic fashion that allows the independent design and optimization of MOFs and SMMs prior to their self-assembly into SMM@MOF composite materials, which features a significant advantage over the more restricted node approach.

Herein we report a route to successfully arranging SMMs of **1** into the multidimensional MOF matrix of **2** under mild conditions. The new magnetic composite Mn_{12}Ac@MOF (**3**) contains exactly one molecule per pore in a long-range ordered crystalline matrix (albeit with not full loading) and fully retains its unique SMM properties while showing a significantly enhanced thermal stability (Figure 1B). This arrangement is advantageous for addressing single magnetic moments in potential SMM-based ultrahigh-density data storage systems.

In order to optimize the Mn_{12}Ac incorporation into the mesoporous MOF host, different reaction conditions were explored. The loading was first performed by soaking **2** in a saturated acetonitrile solution of **1**. This reaction mixture was stirred at room temperature for 12 h. The resulting composite was removed by filtration and carefully washed with acetonitrile to eliminate any residual Mn_{12}Ac molecules outside the MOF. It was subsequently found that longer reaction times (from 24 h up to 1 week) and even heating (from 50 °C up to refluxing) does not significantly affect the loading process. The EDX analyses yielded consistent Mn:Al atomic ratios of approximately 20:80 in all of the prepared Mn_{12}Ac@MOF composites (see section S3 in the Supporting Information (SI)), corresponding to a 2.1 mol% insertion of **1** into **2**. It is worth noting that this value is slightly higher than what was reported for Mn_{12}Ac@silica composites.[13,14]

Four independent experiments were performed all of which verify that **1** is effectively adsorbed within the pores of **2** based on synchrotron-based powder diffraction (SPD) data combined with investigations on the difference envelope density (DED), physisorption analysis (BET surface area and pore size distribution), thermal analyses (TGA and DSC), and in-depth magnetic characterization. The SPD pattern of **3** does not exhibit any shift of its reflections as compared to **2**, and, most importantly, reflections ascribed to **1** or other additional species are absent as evidenced from the high-quality final Le Bail refinements (Figure 2A). These results support the conclusion

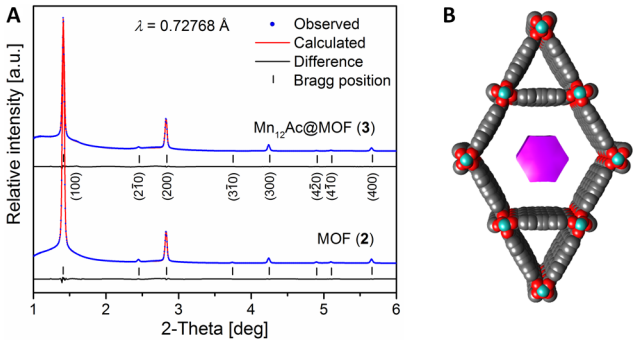

Figure 2. (A) Final Le Bail whole pattern decomposition plots of the activated MOF host **2** (lower) and the composite **3** (upper). (B) Observed structure difference envelope density of **3** ($\rho_\Delta = \rho_{composite} - \rho_{MOF}$, shown in violet) overlapped with a structural model of the host **2**.

that there is no SMM crystallization on the surface or within the pores of **2**. Furthermore, as compared to **2**, a significant reduction in the intensity of the (100) reflection at ∼1.4° 2θ is observed (ca. 50%) in **3**, which is attributed to the fact that insertion of scatterers into the pores leads to an increased phase cancellation between scattering from the framework and the pore regions. This observation enables the generation of structure envelopes for **2** and **3** generated from SPD data (SI, Figure S5).[31,32] Their DED clearly shows a hexagonal-shaped density of 11.6 Å diameter as the most intense feature within the center of the mesopores, which is attributed to the high electron density metal cluster core of **1** (Figure 2B). The central nature of this adsorption site leads us to conclude that any specific interactions with the pore walls can be excluded and that only a single SMM molecule is adsorbed in the transverse direction of the pores (see section S4 in the SI for details on DED analysis).

Nitrogen adsorption isotherms reveal a reversible type IV behavior with one well-defined step at intermediate partial pressures which corresponds to the capillary condensation inside the mesopores (Figure 3A). The BET surface area shows a decrease from 2978.3 $m^2\ g^{-1}$ in **2** to 2085.8 $m^2\ g^{-1}$ in **3**, along with a reduction in the N_2 uptake from ∼1200 to 800 $cm^3\ g^{-1}$ STP. The pore size distribution derived from DFT calculations indicates two types of pores, namely micropores (15.0 Å) and mesopores (26.4 Å), results that are consistent with reported data (Figure 3B).[25] Upon loading of **1** into **2**, a significant reduction in the pore volume of the mesopores from 1.70 $cm^3\ g^{-1}$ in **2** to 1.18 $cm^3\ g^{-1}$ in **3** is observed, whereas the micropores remain unchanged (Figures 3B). This indicates that **1** is solely loaded into the mesopores of **2** as expected due to size exclusion, which is in agreement with the DED analysis (Figure 2B).

Thermogravimetric analysis of **1** reveals that the cluster gradually decomposes upon heating to 350 °C with a total mass loss of 50.3%, which is in good agreement with the reported

DOI: 10.1021/jacs.5b06002
J. Am. Chem. Soc. 2015, 137, 9254−9257

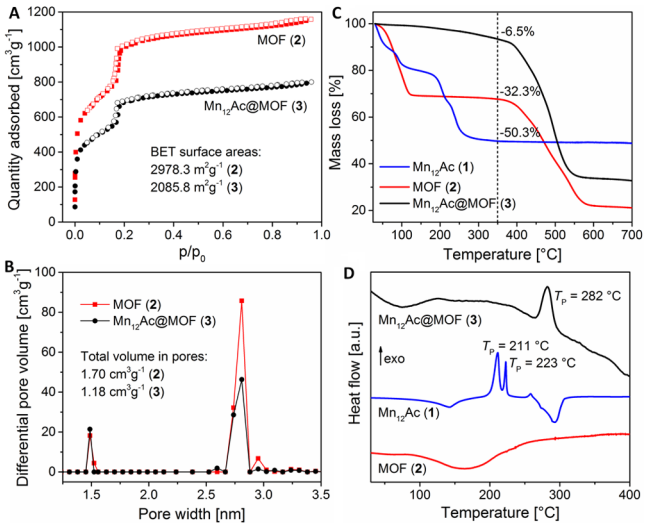

Figure 3. (A) N_2 adsorption (filled symbols) and desorption (open symbols) isotherm collected at 77 K. (B) Density functional theory (DFT) pore size distributions by differential pore volume. Data points of **2** and **3** are shown as red squares and black circles, respectively. (C) TGA and (D) DSC curves for the precursors **1** (blue) and **2** (red), and the composite **3** (black).

data (Figure 3C, blue curve).[25] The decomposition is accompanied by two pronounced exothermic events in the DSC curve (Figure 3D, blue curve). Upon heating **2** to 130 °C, a well-defined mass loss step is observed in the TGA curve (Figure 3C, red curve) which is attributed to the loss of two DMF molecules [Δm_{exp} = 32.3% vs Δm_{calc}(2DMF) = 32.0%] before decomposition, which is observed at 350 °C. The composite **3** shows a significantly different thermal behavior as compared to its precursors; specifically upon heating to 350 °C, a mass loss of only 6.5% was observed, which is in excellent agreement with the 50.3% decomposition of 2.1 mol% of **1** [Δm_{calc}(50.3% of 2.1 mol% Mn_{12}Ac) = 6.5%]. No additional solvent molecules are incorporated into the framework (Figure 3C, black curve). Based on the 2.1 mol% loading and the latter observation, it can be assumed that the channel pores of **2** are loaded with **1** only at the periphery of the bulk crystals, thereby preventing solvent molecules to enter the remaining internal pores. This surface nanostructuring effect could be advantageous for addressing individual SMM molecules in potential applications, rather than having crystallographically ordered SMM molecules within the entire MOF crystals. Most importantly, the associated exothermic DSC signal for the decomposition of **1** is shifted to higher temperatures (~280 °C) as compared to the free molecules (~210 °C) (Figure 3D, black curve). These data indicate that the confinement of **1** within the nanoscopic cavities of **2** significantly enhances its thermal stability whereas the overall framework stability remains unchanged.

Furthermore, a series of rigorous control experiments were performed on a physical mixture of **1** and **2** with identical atomic Al:Mn ratios as found in **3**. The same experimental conditions as described above led to an exact overlay of their individual diffraction, adsorption and thermal behaviors as opposed to the composite (SI, Figures S6–S8). These additional experiments further support the successful formation of the composite material **3**.

The magnetic properties of **3** were extensively investigated. It should be noted that only the "as-synthesized" form of **3** was characterized, as the activated form does not retain SMM behavior upon thermal activation. The temperature and frequency dependence of the ac susceptibility data were measured under a zero dc field over the frequency range of 1–1500 Hz. An obvious frequency dependence of the out-of-phase ac susceptibility (χ'') was observed with peaks in the range 3.4–5.8 K which shift to higher temperatures as the frequency increases, a result that is typical of the slow relaxation of the magnetization of **1** (Figure 4A).[23] These results support

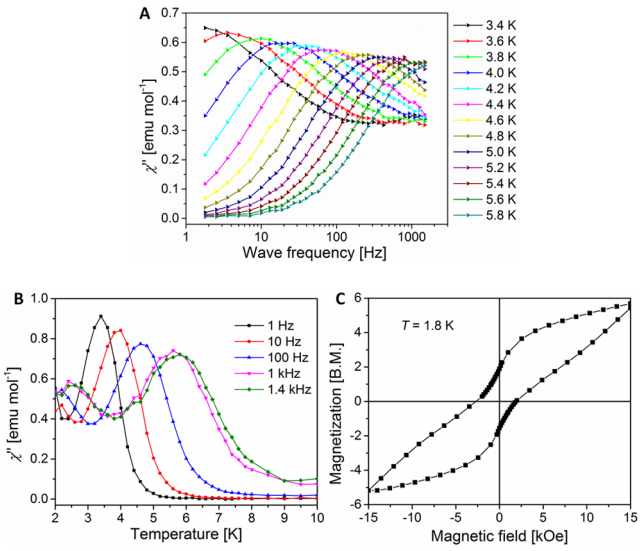

Figure 4. (A) Frequency dependence of the out-of-phase ac magnetic susceptibility at different temperatures. (B) Temperature dependence of the out-of-phase ac magnetic susceptibility at different ac frequencies. (C) Field-dependent hysteresis of the magnetization.

the contention that the Mn_{12}Ac molecules have been preserved during their incorporation into the MOF cavities. A fitting of the χ'' peak temperatures at the corresponding frequencies to the Arrhenius law, $\tau = \tau_0 \exp(\Delta E/k_B T)$, reveals an effective energy barrier of $\Delta E/k_B \approx 57$ K and a pre-exponential factor of $\tau_0 \approx 5.2 \times 10^{-9}$ s (SI, Figure S9). A control sample of **1** was also studied to ascertain the influence of the MOF on the SMM properties, the results of which are $\Delta E/k_B \approx 70$ K and $\tau_0 \approx 1.2 \times 10^{-8}$ s (SI, Figure S10). The slight change in properties is not surprising given the absence of crystallizing solvent molecules (four water and two acetic acid molecules) and the different chemical environment of the SMM molecules within the MOF pores. Similar values were reported for other Mn_{12} composites, such as SMM@porous silicas (72 K/1.03 × 10^{-8} s,[13] 63 K/4.06 × 10^{-9} s,[14] and 58.4 K/1.3 × 10^{-8} s[15]) and SMM@carbon nanotubes (57.0 K/9.4 × 10^{-9} s[11]).

In addition, a minor and faster relaxation process was observed in both **1** (SI, Figure S12) and **3** (Figure 4B) below 3 K which is attributed to an isomer of **1** with a different Jahn–Teller distortion direction of the Mn(III) ions as reported previously. We note that this process is more prominent in **3**, which may originate from the loss of solvent molecules.[33]

Variable-temperature dc magnetic measurements of **3** at 1000 Oe also exhibit typical behavior for Mn_{12}Ac derivatives (SI, Figure S11).[15] Field-dependent magnetization of **3** exhibits an obvious hysteresis loop with a coercive field of ~2000 Oe (Figure 4C). A narrowing of the hysteresis loop at low fields is consistent with the presence of quantum tunneling of the magnetization and the presence of the faster relaxation isomer

DOI: 10.1021/jacs.5b06002
J. Am. Chem. Soc. 2015, 137, 9254–9257

of $Mn_{12}Ac$. The magnetic properties of other reported porous $Mn_{12}Ac$ composite materials (carbon nanotubes and silicas) are discussed in the context of these results in the SI, section S6.

In summary, the results reported in this study indicate that it is possible to incorporate the SMM $Mn_{12}Ac$ into a mesoporous MOF host. It has been demonstrated that the sufficiently large pore size and unreactive interior of the framework facilitates the insertion and preservation of the SMM's unique magnetic properties. Most importantly, we have shown that SMM loading occurs only at the periphery of the bulk MOF crystals with a single SMM cluster in the transverse direction of the pores to yield a long-range ordered crystalline composite material with significantly enhanced thermal stability. We believe that these findings will pave the way for new venues for the development of novel advanced high-density information storage devices.

■ ASSOCIATED CONTENT

Supporting Information

Synthetic procedure and details on various methods, general analytical techniques, EDX and TEM analysis, synchrotron-based structure envelope studies, control experiments using a physical mixture, magnetic characterization, and PXRD and IR data. The Supporting Information is available free of charge on the ACS Publications website at DOI: 10.1021/jacs.5b06002.

■ AUTHOR INFORMATION

Corresponding Author

*mwriedt@clarkson.edu

Author Contributions

‖D.A. and J.B.P. contributed equally to this work.

Notes

The authors declare no competing financial interest.

■ ACKNOWLEDGMENTS

We gratefully acknowledge Clarkson University for their generous start-up funding. J.B.P. thanks the Center of Advanced Material Processing at Clarkson University for an undergraduate summer research stipend in 2014. Work carried out at the Advanced Photon Source at Argonne National Laboratory was supported by the U.S. Department of Energy, Office of Science, Office of Basic Energy Sciences, under Contract No. DE-AC02-06CH11357. The magnetic measurements were conducted in the Department of Chemistry SQUID Facility at Texas A&M University with a magnetometer obtained by a grant from the National Science Foundation (CHE-9974899). The magnetic work in this study was performed by K.R.D.'s group and was funded by the Division of Chemical Sciences, Geosciences, and Biosciences, Office of Basic Energy Sciences, of the U.S. Department of Energy through Grant DE-SC0012582. K.R.D. also thanks the Robert A. Welch Foundation (Grant A-1449) for summer salary for X.Z.

■ REFERENCES

(1) Bagai, R.; Christou, G. *Chem. Soc. Rev.* **2009**, *38*, 1011.
(2) Layfield, R. A. *Organometallics* **2014**, *33*, 1084.
(3) Woodruff, D. N.; Winpenny, R. E. P.; Layfield, R. A. *Chem. Rev.* **2013**, *113*, 5110.
(4) Walter, C. *Sci. Am.* **2005** (July), http://www.scientificamerican.com/article/kryders-law/.
(5) Ritter, S. K. *Chem. Eng. News* **2004**, *82* (50), 29.
(6) Bogani, L.; Wernsdorfer, W. *Nat. Mater.* **2008**, *7*, 179.
(7) Domingo, N.; Bellido, E.; Ruiz-Molina, D. *Chem. Soc. Rev.* **2012**, *41*, 258.
(8) Cornia, A.; Mannini, M.; Sainctavit, P.; Sessoli, R. *Chem. Soc. Rev.* **2011**, *40*, 3076.
(9) Gomez-Segura, J.; Veciana, J.; Ruiz-Molina, D. *Chem. Commun.* **2007**, 3699.
(10) Bogani, L.; Danieli, C.; Biavardi, E.; Bendiab, N.; Barra, A.-L.; Dalcanale, E.; Wernsdorfer, W.; Cornia, A. *Angew. Chem., Int. Ed.* **2009**, *48*, 746.
(11) del Carmen Giménez-López, M.; Moro, F.; La Torre, A.; Gómez-García, C. J.; Brown, P. D.; van Slageren, J.; Khlobystov, A. N. *Nat. Commun.* **2011**, *2*, 407.
(12) Pardo, E.; Burguete, P.; Ruiz-Garcia, R.; Julve, M.; Beltran, D.; Journaux, Y.; Amoros, P.; Lloret, F. *J. Mater. Chem.* **2006**, *16*, 2702.
(13) Willemin, S.; Arrachart, G.; Lecren, L.; Larionova, J.; Coradin, T.; Clerac, R.; Mallah, T.; Guerin, C.; Sanchez, C. *New J. Chem.* **2003**, *27*, 1533.
(14) Coradin, T.; Larionova, J.; Smith, A. A.; Rogez, G.; Clérac, R.; Guérin, C.; Blondin, G.; Winpenny, R. E. P.; Sanchez, C.; Mallah, T. *Adv. Mater. (Weinheim, Ger.)* **2002**, *14*, 896.
(15) Clemente-Leon, M.; Coronado, E.; Forment-Aliaga, A.; Amoros, P.; Ramirez-Castellanos, J.; Gonzalez-Calbet, J. M. *J. Mater. Chem.* **2003**, *13*, 3089.
(16) Saywell, A.; Magnano, G.; Satterley, C. J.; Perdigão, L. M. A.; Britton, A. J.; Taleb, N.; del Carmen Giménez-López, M.; Champness, N. R.; O'Shea, J. N.; Beton, P. H. *Nat. Commun.* **2010**, *1*, 75.
(17) Voss, S.; Fonin, M.; Rüdiger, U.; Burgert, M.; Groth, U.; Dedkov, Y. S. *Phys. Rev. B: Condens. Matter Mater. Phys.* **2007**, *75*, 045102.
(18) Zhou, H.-C.; Long, J. R.; Yaghi, O. M. *Chem. Rev.* **2012**, *112*, 673.
(19) Zhou, H.-C.; Kitagawa, S. *Chem. Soc. Rev.* **2014**, *43*, 5415.
(20) Zhu, Q.-L.; Xu, Q. *Chem. Soc. Rev.* **2014**, *43*, 5468.
(21) Falcaro, P.; Ricco, R.; Doherty, C. M.; Liang, K.; Hill, A. J.; Styles, M. J. *Chem. Soc. Rev.* **2014**, *43*, 5513.
(22) Lu, G.; Li, S.; Guo, Z.; Farha, O. K.; Hauser, B. G.; Qi, X.; Wang, Y.; Wang, X.; Han, S.; Liu, X.; DuChene, J. S.; Zhang, H.; Zhang, Q.; Chen, X.; Ma, J.; Loo, S. C. J.; Wei, W. D.; Yang, Y.; Hupp, J. T.; Huo, F. *Nat. Chem.* **2012**, *4*, 310.
(23) Caneschi, A.; Gatteschi, D.; Sessoli, R.; Barra, A. L.; Brunel, L. C.; Guillot, M. *J. Am. Chem. Soc.* **1991**, *113*, 5873.
(24) Lis, T. *Acta Crystallogr., Sect. B: Struct. Crystallogr. Cryst. Chem.* **1980**, *36*, 2042.
(25) Lo, S.-H.; Chien, C.-H.; Lai, Y.-L.; Yang, C.-C.; Lee, J. J.; Raja, D. S.; Lin, C.-H. *J. Mater. Chem. A* **2013**, *1*, 324.
(26) Katsenis, A. D.; Brechin, E. K.; Papaefstathiou, G. S. *Encyclopedia of Inorganic and Bioinorganic Chemistry*; John Wiley & Sons, Ltd.: New York, 2011.
(27) Chen, M.; Sañudo, E. C.; Jiménez, E.; Fang, S.-M.; Liu, C.-S.; Du, M. *Inorg. Chem.* **2014**, *53*, 6708.
(28) Mahata, P.; Natarajan, S.; Panissod, P.; Drillon, M. *J. Am. Chem. Soc.* **2009**, *131*, 10140.
(29) Zhang, X.; Vieru, V.; Feng, X.; Liu, J.-L.; Zhang, Z.; Na, B.; Shi, W.; Wang, B.-W.; Powell, A. K.; Chibotaru, L. F.; Gao, S.; Cheng, P.; Long, J. R. *Angew. Chem., Int. Ed.* **2015**, DOI: 10.1002/anie.201503636.
(30) Zhou, Q.; Yang, F.; Xin, B.; Zeng, G.; Zhou, X.; Liu, K.; Ma, D.; Li, G.; Shi, Z.; Feng, S. *Chem. Commun.* **2013**, *49*, 8244.
(31) Yakovenko, A. A.; Wei, Z.; Wriedt, M.; Li, J.-R.; Halder, G. J.; Zhou, H.-C. *Cryst. Growth Des.* **2014**, *14*, 5397.
(32) Wriedt, M.; Sculley, J. P.; Yakovenko, A. A.; Ma, Y.; Halder, G. J.; Balbuena, P. B.; Zhou, H.-C. *Angew. Chem., Int. Ed.* **2012**, *51*, 9804.
(33) Sun, Z.; Ruiz, D.; Hendrickson, D. N.; Dilley, N. R.; Brian Maple, M.; Soler, M.; Folting, K.; Christou, G.; Ribas, J. *Chem. Commun.* **1999**, 1973.

DOI: 10.1021/jacs.5b06002
J. Am. Chem. Soc. 2015, 137, 9254−9257